# Enhanced Electrochemical Performance of a Ti−Cr-Doped LiMn$_{1.5}$Ni$_{0.5}$O$_4$ Cathode Material for Lithium-Ion Batteries

Yiyuan Luo, Zhou Cui, Changxu Wu, Baisheng Sa, Cuilian Wen,* Hengyi Li,* Jianping Huang, Chao Xu, and Zhengbing Xu*

Read Online

ACCESS | Metrics & More | Article Recommendations

**ABSTRACT:** Ti, Cr dual-element-doped LiMn$_{1.5}$Ni$_{0.5}$O$_4$ (LNMO) cathode materials (LTNMCO) were synthesized by a simple high-temperature solid-phase method. The obtained LTNMCO shows the standard structure of the $Fd\bar{3}m$ space group, and the Ti and Cr doped ions may replace the Ni and Mn sites in LNMO, respectively. The effect of Ti−Cr doping and single-element doping on the structure of LNMO was studied by X-ray diffraction (XRD), Fourier transform infrared (FT-IR), X-ray photoelectron spectroscopy (XPS), and scanning electron microscopy (SEM) characteristics. The LTNMCO exhibited excellent electrochemical properties with a specific capacity of 135.1 mAh·g$^{-1}$ for the first discharge cycle and a capacity retention rate of 88.47% at 1C after 300 cycles. The LTNMCO also has high rate performance with a discharge capacity of 125.4 mAh·g$^{-1}$ at a 10C rate, 93.55% of that at 0.1C. In addition, the CIV and EIS results show that the LTNMCO showed the lowest charge transfer resistance and the highest diffusion coefficient of lithium ions. The enhanced electrochemical properties may be due to a more stable structure and an optimized Mn$^{3+}$ content in LTNMCO through TiCr doping.
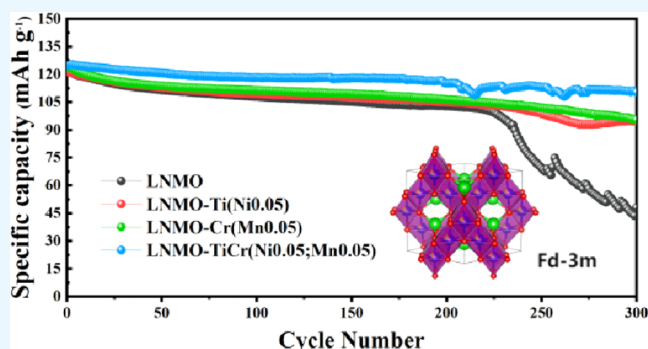
## 1. INTRODUCTION

Cathode materials with better electrochemical performance for Li-ion batteries (LIBs) need to be investigated to accommodate different applications such as EV, HEV, and portable electronic devices. Although the theoretical specific capacity (∼147 mAh·g$^{-1}$) of LiMn$_{1.5}$Ni$_{0.5}$O$_4$ (LNMO) is lower compared to that of conventional layer cathode materials (LCO, NCM, etc.), LNMO is believed to be a new generation of high-performance cathodes due to its high energy density (658 Wh·kg$^{-1}$), high working voltage (∼4.7 V vs Li/Li+), and low cost.[1−5] In general, LNMO is reported to have two crystal structures depending on the Ni/Mn arrangement including ordered P4$_3$32 and disordered $Fd\bar{3}m$,[6] which can be controlled by the synthesis process.[7] Between the two structures, the LNMO with the $Fd\bar{3}m$ structure was found to have better electrochemical performance because of its distinct lithium-ion diffusion channels, but there are still some barriers for the commercial application of LNMO. First is the difficulty of synthesizing pure $Fd\bar{3}m$ LNMO.[8,9] The second is the low bulk phase ionic conductivity of LNMO caused by the octahedral vacancies transfer mechanism of Li ions in the spinel structure.[5,10] The third is the dissolution of Mn ions in the electrolyte due to the Jahn−Teller effect, leading to the degradation of electrochemical properties.[11−13] The last is

related to the inevitable reaction between electrode and electrolyte at a high cutoff voltage during the long cycle.[14]

To solve the above problems, much effort has been made to improve the structural stability and electrochemical performances of LNMO such as elemental doping, surface coating, and morphology control. Among them, doping modification is a simple and efficient research method; for example, some amounts of Al, Ti, Mg, Cr, Fe, Zr, Cu, F, Cl, S, etc. have been used for the substitution of Ni sites, Mn sites, O sites, or multiple sites of LNMO.[12,15−23] Chen et al. used a rapid precipitation and hydrothermal method to synthesize Al-doped LiNi0.5Mn1.5O4 cathode materials with the first circle capacity of 126.8 mAh·g$^{-1}$ at 0.5C and the capacity retention rate of 87% after 200 cycles. The doping Al ion could increase the activation energy of Li, thus further enhancing the diffusion rate of lithium ions,[24] but single-element doping is not sufficient to prevent the degradation of material properties at a
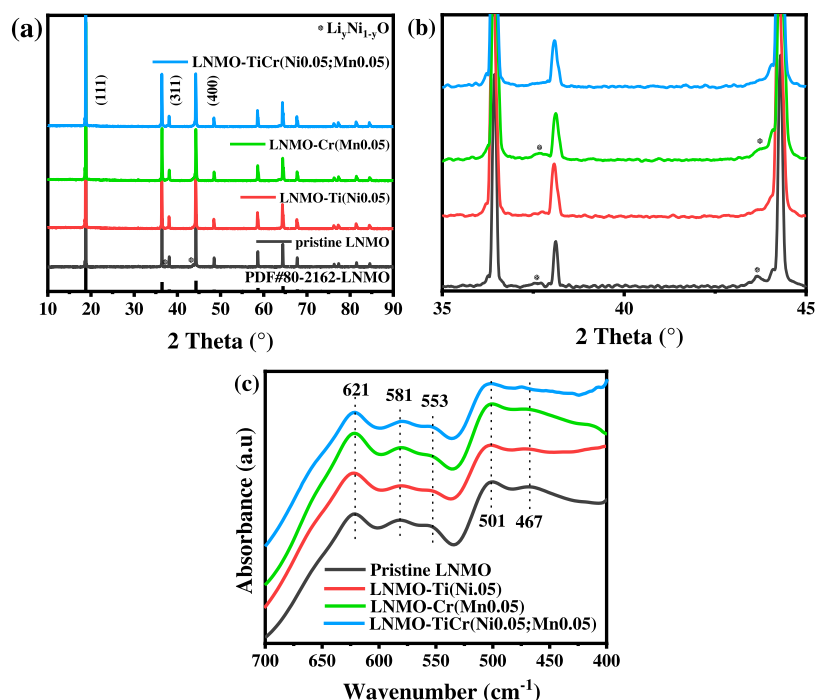
**Figure 1.** (a) XRD patterns of all samples compared with standard LNMO XRD patterns. (b) Enlarged view around 35−45°.(c) FT-IR spectra of all samples.

higher voltage. The Cu and Al codoped $LiNi_{0.5}Mn_{1.5}O_4$ cathode materials synthesized by the high-temperature solid-phase method showed capacity retention of 103.4 mAh·g$^{-1}$ and 96.55% at 5C compared with that at 0.25C after 100 cycles, which is attributed to the rich Cu on the surface to protect the interface and inhibit side reactions.[25] The $Mg^{2+}/F^-$ codoped $LiNi_{0.5}Mn_{1.5}O_4$ cathode materials obtained from the solid-phase method have a better capacity retention rate of 86.2% after 400 charge/discharge cycles at 5C, which is due to the more stable structure, better crystallinity, and higher diffusion coefficient of lithium ions after doping.[26] However, the electrochemical performance of doping LNMO at high temperatures is still low, which is needed to be addressed in future research.

In this work, we synthesized Ti−Cr-doped LNMO, Ti-doped LNMO, Cr-doped LNMO, and pristine LNMO by solid-phase for comparative study. The effect of Ti−Cr doping and single-element doping on structure, capacities, rate, and long cycles performance is examined. Accordingly, the electrochemical performance is further studied and the possible Ti−Cr doping mechanism in LNMO is discussed.

## 2. EXPERIMENTAL SECTION

**2.1. Synthesis of Materials.** Synthesis of pristine LNMO and doped samples using a solid-state reaction. Mixed 1.0617 g $Li_2CO_3$, 1.0221 g NiO, and 2.9122 g MnO according to the mass fraction of 1.05:0.5:1.5 in ethanol and perform ball mill at a speed of 400 rpm for 5 h. The mixed slurry was transferred to an oven at 110 °C for 12 h to dry the powder, then materials were preheated at 500 °C for 5 h and annealed at 950 °C for 15 h in an air atmosphere. Grind the powder until it has no obvious granularity and after sieving with 200 mesh, $LiNi_{0.5}Mn_{1.5}O_4$ cathode material is obtained. Doped samples of $LiTi_{0.05}Ni_{0.45}Mn_{1.5}O_4$ (LTNMO), $LiNi_{0.5}Mn_{1.45}Cr_{0.05}O_4$

(LNMCO), and $LiTi_{0.05}Ni_{0.45}Mn_{1.45}Cr_{0.05}O_4$ (LTNMCO) were prepared in the same way.

**2.2. Materials Characterization.** For the confirmation and analysis of the crystal structure by X-ray diffraction (XRD, Rigaku MiniFlex600) with Cu Kα radiation, the diffraction patterns were collected in the range of $2\theta = 10−90°$ at a scan speed of 5°/min. The Rietveld refinement of the XRD data was processed through GSAS II. For further confirmation of the space group of the material, Fourier transform infrared spectroscopy (FITR, Nicolet 5700) was performed. The observation of material morphology and size was performed by a scanning electron microscope (SEM, ZEISS SUPRA 55). The chemical composition and elemental analysis of materials were performed by EDX mapping equipped in the SEM and X-ray photoelectron spectroscopy (XPS, Thermo Scientific ESCALAB 250).

**2.3. Electrochemical Measurements.** The cathode slurry consists of 90:5:5 wt % active material, Super-P, and poly(vinylidene fluoride) (PVDF) in N-methyl pyrrolidone (NMP). The mixture is mixed well by centrifuging three times; then, the slurry is evenly scraped onto the aluminum foil and transferred to a vacuum oven. The mass of the active material is about 6−7 mg. The half-cells are assembled in a glovebox with an Ar-filled atmosphere. The LNMO cathode material, Celgard 2400, an electrolyte of 1 mol·L$^{-1}$ $LiPF_6$ in 3:7 EC/DEC, and lithium foil anode are put into the CR2025 battery case to prepare the coin cells. The charge/discharge measurement was tested in a 3.2−4.95 V range of voltage with the neware CT-4008 battery test system (1C = 147 mAh·g$^{-1}$). Cyclic voltammetry (CV) was performed between 3.5 and 4.5 V with a scan rate of 0.05 mV·s$^{-1}$. Electrochemical impedance spectroscopy (EIS) tests were performed in the frequency range between 10 mHz and 100 kHz with an amplitude of 5 mV.
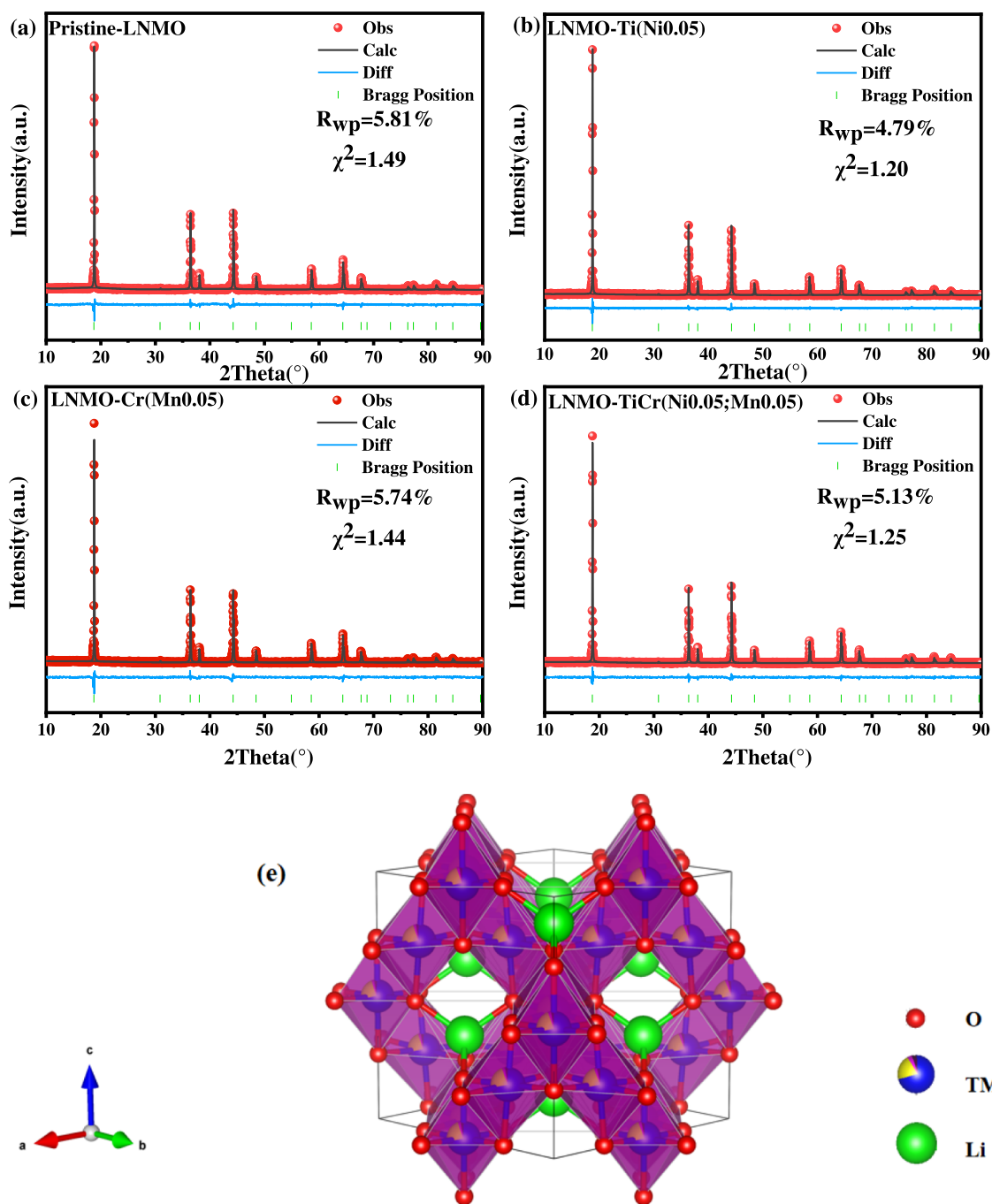
**Figure 2.** Rietveld refinement of (a) pristine LNMO; (b) LNMO-Ti(Ni0.05); (c) LNMO-Cr(Mn0.05); and (d) LNMO-TiCr(Ni0.05;Mn0.05). (e) Crystal structure of LNMO.

## 3. RESULTS AND DISCUSSION

Powder XRD patterns of pristine $LiNi_{0.5}Mn_{1.5}O_4$ and doping samples are compared in Figure 1a, with the narrow and sharp diffraction peaks showing well crystallinity of all samples. The main diffraction peaks matched perfectly with the standard card of cubic spinel $LiNi_{0.5}Mn_{1.5}O_4$ cathode material (PDF#80-2162), indicating no main structure change of LNMO by a small amount of elemental doping. More details of the XRD patterns from 35 to 45° are shown in Figure 1b, two very small peaks can be found at 37.5 and 43.7° in the LNMCO as well as pristine LNMO, which may be due to the inevitable formation of $Li_yNi_{1−y}O$ rock salt phase during the synthesis process. When annealed over 600 degrees, the

impure phases are inevitably generated. It allows LNMO to produce a large number of oxygen vacancies, allowing some of the Mn ions to exist as 3+ to compensate for the loss of oxygen. This is the main source of $Mn^{3+}$ in the material.[27,28] The formation of $Li_yNi_{1−y}O$ in LNMCO suggests that the doping Cr only occupies the Mn site, which is different from the previously reported 16d Ni/Mn sites with Cr simultaneously doped with LNMO.[29,30] However, no significant impurity peaks appear in the single-doped Ti and Ti−Cr dual-doped samples. It may be because the Ti ions play a key role in stabilizing the structure of the material owing to their strong oxidation properties, allowing the surrounding oxygen ions to hold more electrons to enhance the Ni/Mn−O ionic bond.[31]

Figure 1c shows the FT-IR spectrum of LNMO, providing more details for analyzing the cation ordering of doping LNMOs. All samples have five similar distinct peaks at 621, 581, 553, 501, and 467 cm$^{-1}$, which belong to the $Fd\bar{3}m$ disordered structure. The intensity of the 581 cm$^{-1}$ Ni–O band of LTNMO and LNMCO decreases after Ti doping due to the decreased ordering degree of the cation at the 16d octahedral site.[32] The intensity ratios of I(621)/I(581) corresponding to the degree of disorder for LNMO, LTNMO, LNMCO, and LTNMCO are 1.055, 1.077, 1.073, and 1.066 respectively. The increase in the degree of disorder for the doping samples may come from more Mn$^{3+}$ existing in the materials.[33] For the Ti–Cr doping sample, the degree of disorder is between the pristine LNMO and single doping LNMO materials, suggesting that the amount of Mn$^{3+}$ in LTNMCO may be more beneficial to enhance the electrochemical properties. This is mainly due to the Mn$^{3+}$ accompanying oxygen vacancies, which can improve the diffusion of Li ions within the material Mn$^{3+}$ and increase the electrical conductivity[34–36]

Rietveld refinements XRD data is shown in Figure 2a–d. The diffraction peaks of all materials correspond to the PDF card (JCPDS No. 80-2162). It indicates that the material mainly consists of the disordered phase of LNMO (the crystal structure of the material is shown in Figure 2e).[37,38] The relatively reliable lattice parameters obtained by Rietveld refinement patterns are listed in Table 1. The lattice

**Table 1. Lattice Parameters of LNMO, LNMO-Ti(Ni0.05), LNMO-Cr(Mn0.05) and LNMO-TiCr(Ni0.05; Mn0.05) Materials**

| sample | $a = b = c$ (Å) | $V$ (Å) | $I_{(311)}/I_{(400)}$ |
|---|---|---|---|
| LNMO | 8.1684 | 545.02 | 0.982 |
| LNMO-Ti(Ni0.05) | 8.1836 | 548.06 | 1.048 |
| LNMO-Cr(Mn0.05) | 8.1732 | 545.98 | 1.074 |
| LNMO-TiCr(Ni0.05;Mn0.05) | 8.1787 | 547.09 | 0.964 |

parameters are 8.1684, 8.1836, 8.1732, and 8.1787 Å for pristine LNMO, LTNMO, LNMCO, and LTNMCO, respectively. The increase in lattice parameters of LTNMO, LNMCO, and LTNMCO compared to that of pristine LNMO is mainly due to the replacement of Ni$^{2+}$ (0.069 nm) and Mn$^{4+}$ (0.053 nm) with larger ions Ti$^{4+}$ (0.0745 nm) and Cr$^{3+}$ (0.069 nm), resulting in the lattice expansion of the material. The intensity ratio of the I(311)/I(400) peak of LTNMCO is 0.964, much lower than those of LTNMO and LNMCO, indicating a lower degree of distortion and higher structural stability,[39,40] probably due to stronger Ti–O and Cr–O than Ni–O and Mn–O bonding energies, contributing positively to the structure stability after Ti doping into the material. The intensity ratio of I(311)/I(400) also indicates that the transition metal tends to occupy the 8a position of Li ions more due to the presence of impure phases.[32,41] The maximum I(311)/I(400) ratio of 1.074 for LNMCO may be caused by the pure presence of Li$_y$Ni$_{1-y}$O, which hinders the diffusion of Li ions.

The effect of the change of elemental valence on the material after doping was investigated by XPS. From the XPS spectra of Mn 2p$_{3/2}$ and Mn 2p$_{1/2}$ for all samples in Figure 3a–d, two well-fitted peaks can be observed. The peaks at 642 and 653.6 eV are assigned to Mn$^{3+}$ and those at 643.3 and 654.8 eV are assigned to Mn$^{4+}$. The relative content of Mn$^{3+}$ and Mn$^{4+}$

calculated from the peak area is listed in Table 2. As listed in Table 2, the doping of Cr leads to a reduction in Mn$^{3+}$ for LNMCO (32.54%), indicating that the Mn ion should keep the valence state of +4 to achieve charge balance in LNMCO as well as the decrease of Mn$^{3+}$ can restrain the Jahn–Teller effect and prevent the dissolution of metal ions.[32] For comparison, LTNMO has the largest amount of Mn$^{3+}$ (40.32%), probably due to the increased disorder of the material. The Mn$^{3+}$ content of LTNMCO is between that of pristine LNMO and single-doped samples, corresponding to the FT-IR results. A certain amount of Mn$^{3+}$ can improve the electrochemical properties of the material, but too much Mn$^{3+}$ will lead to severe disproportionation reactions.[42] As can be seen from the XPS spectra of Ni for LNMO and LTNMCO in Figure 3e,f, the peaks at 872.3 and 854.7 eV are assigned to Ni$^{2+}$ 2p$_{3/2}$ and Ni$^{2+}$ 2p$_{1/2}$, respectively. Additionally, the chemical state of Ti and Cr in the LTNMCO sample was demonstrated by the XPS spectra of Ti 2p and Cr 2p shown in Figure 3g,h. The Ti 2p peak at about 458.1 eV is attributed to Ti$^{4+}$ and the Cr 2p peak at about 576.3 eV is attributed to Cr$^{3+}$, which also conforms to the XRD and FT-IR results that the synergistic effect of Ti–Cr doping could help optimize the amount of Mn$^{3+}$ in LNMO.

The SEM images of all samples shown in Figure 4a–d exhibit spinel morphology consisting of aggregates of small octahedral particles, the pristine LNMO has more crystalline unformed particles, which indicates less complete crystallization. The LTNMO and LNMCO samples exhibited higher crystallinity and more uniform grain size. The morphology of the LTNMCO sample is different from those of other samples in the sense that the observed surface cut is smooth and clean, indicating the complete crystallization of LTNMCO and facilitating the suppression of adverse reactions at the cathode interface in contact with the electrolyte at high voltages. Furthermore, EDS mapping was conducted on the LTNMCO sample, as shown in Figure 4e–i. The four elements Ni, Mn, Ti, and Cr are distributed well in the sample, indicating that the Ti and Cr elements have successfully entered the spinel material.

In order to investigate the effect of Ti/Cr doping on the discharge capacity of the material, a constant current charge/discharge test was conducted at room temperature (30 °C) with the test voltage range at 3.2–4.95 V and the charge/discharge rate of 0.2C. As shown in Figure 5a, all samples have similar charge/discharge curves with two-stage plateaus. For the $Fd\bar{3}m$ space group LNMO, the oxidation peak of the 4.7 V plateau splits into two independent Ni$^{2+}$/Ni$^{3+}$ and Ni$^{3+}$/Ni$^{4+}$ redox coupling peaks, while the short plateau at 4.0 V corresponds to the Mn$^{3+}$/Mn$^{4+}$ redox couple,[43] implying the existence of Mn$^{3+}$ ions in LNMO. Obviously, the Cr-doped sample has a shorter plateau at 4.0 V than pristine LNMO, indicating less Mn$^{3+}$ in LNMCO, while the plateau at 4.0 V of Ti and Ti–Cr–doped samples is longer, indicating more Mn$^{3+}$ in LTNMO and LTNMCO, which conforms to the XPS results described above. The first cycle discharge capacities of LNMO, LTNMO, LNMCO, and LTNMCO are 127.6, 127.3, 128.5, and 135.1 mAh·g$^{-1}$, respectively. The capacity of the first circle of LTNMCO is much higher than that of pristine LNMO and other single doping samples, which due to the increased lattice parameters and more stable structure of LNMO by Ti–Cr doping forms a larger channel for lithium-ion diffusion and facilitates the transport. Figure 5b,c shows the rate performance tests of the material at room temperature (30
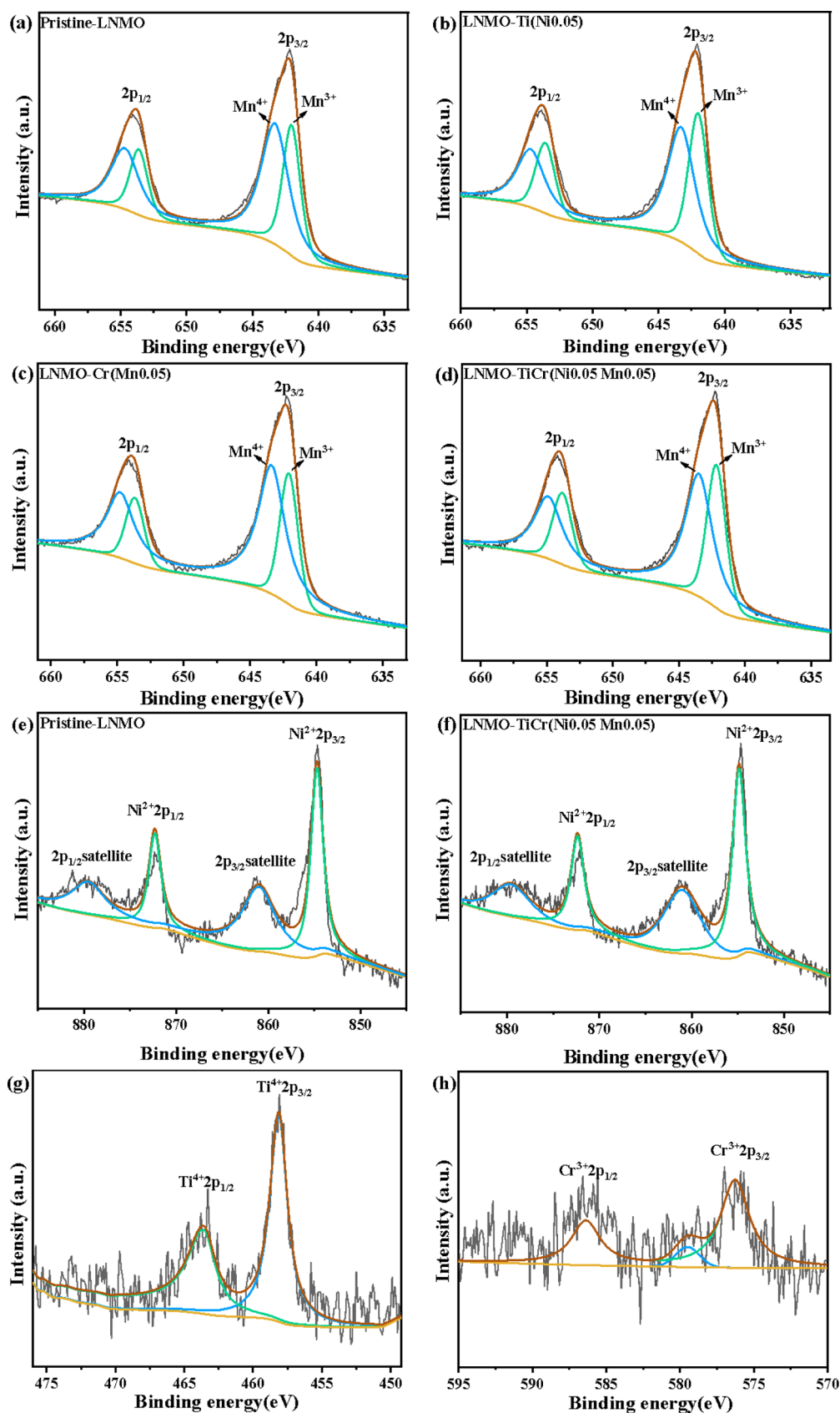
**Figure 3.** XPS spectra of Mn 2p: (a) pristine LNMO; (b) LNMO-Ti(Ni0.05); (c) LNMO-Cr(Mn0.05); and (d) LNMO-TiCr(Ni0.05;Mn0.05). XPS spectra of Ni 2p (e) pristine LNMO and (f) LNMO-TiCr(Ni0.05;Mn0.05). XPS spectra of (g) Ti and (h) Cr elements of the LNMO-TiCr(Ni0.05;Mn0.05) sample.

**Table 2. $Mn^{3+}/Mn^{4+}$ Ratio of LNMO, LNMO-Ti(Ni0.05), LNMO-Cr(Mn0.05), and LNMO-TiCr(Ni0.05; Mn0.05) Materials**

| sample | $Mn^{3+}$ area | $Mn^{4+}$ area | $Mn^{3+}/Mn^{4+}$ |
|---|---|---|---|
| LNMO | 77341.98 | 127878.7 | 37.69%/62.31% |
| LNMO-Ti(Ni0.05) | 84927.72 | 125712.2 | 40.32%/59.68% |
| LNMO-Cr(Mn0.05) | 61317.24 | 127147.8 | 32.54%/67.46% |
| LNMO-TiCr(Ni0.05;Mn0.05) | 64668.66 | 104179.7 | 38.3%/61.7% |
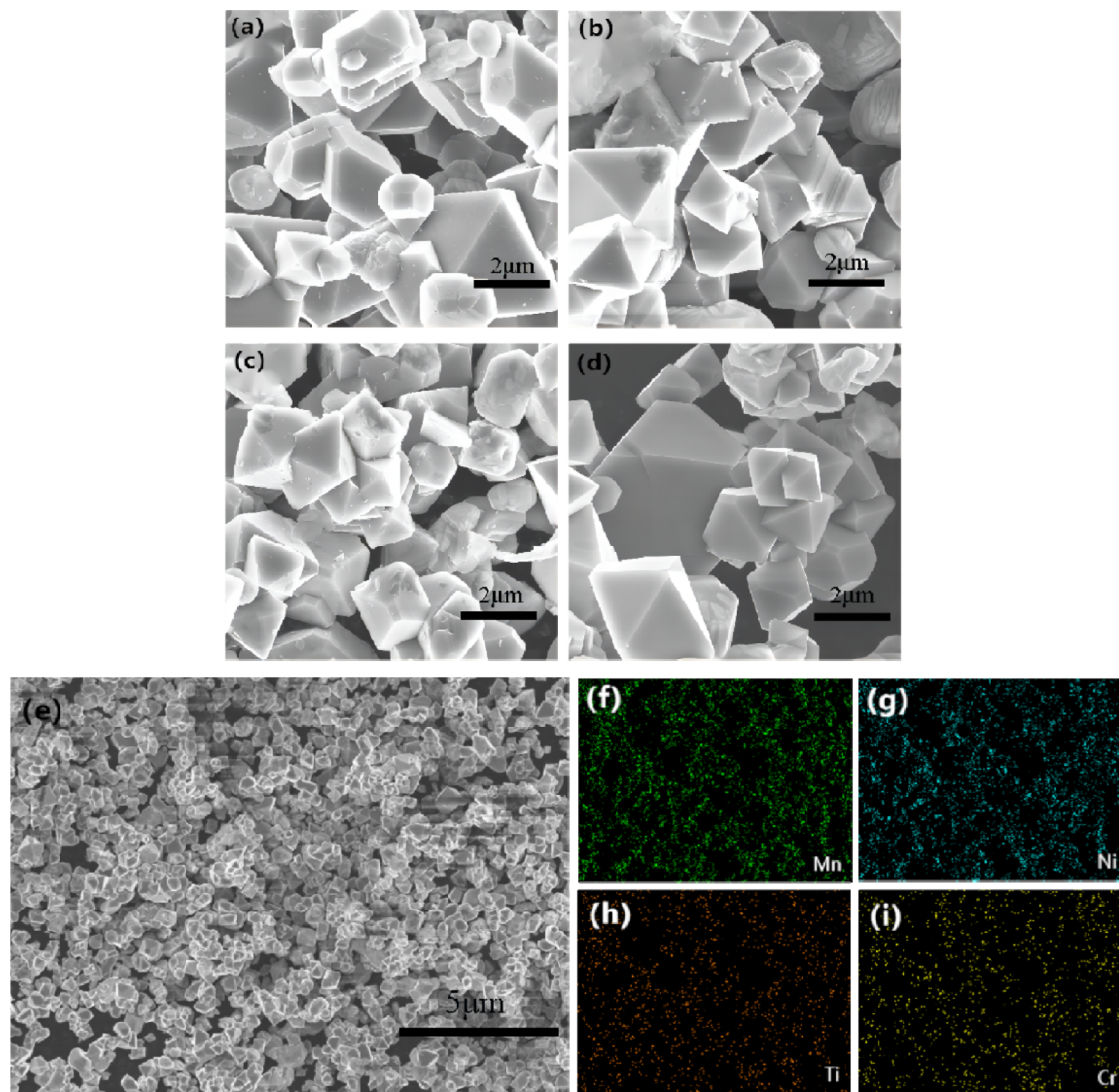


**Figure 4.** SEM images of (a) pristine LNMO; (b) LNMO-Ti(Ni0.05); (c) LNMO-Cr(Mn0.05); and (d) LNMO-TiCr(Ni0.05;Mn0.05). (e–i) EDS mapping image of the LNMO-TiCr(Ni0.05; Mn0.05) material.

°C) and a high temperature (60 °C). The trend of capacity decay with an increased discharge rate of the doped material is smoother than that of the undoped material, especially under the high discharge rate conditions of 5C and 10C, the discharge capacity of the doped material is obviously higher than that of the undoped material. Among them, LTNMCO showed the most remarkable enhancement, with first discharge capacities of 134.0 mAh·g$^{-1}$ at 0.1C and 125.4 mAh·g$^{-1}$ at 10C discharge rate, which has a 93.35% capacity of 0.1C at 10C. However, the discharge capacities of pristine LNMO at 10C is only 83.66% of that at 0.1C. Compared with room temperature, all materials have a decrease in rate performance under high-temperature test conditions. Since the high-temperature working environment leads to accelerated electrolyte decom-

position and increased side reaction products, the unstable flim is generated on the electrode surface, which affects lithium-ion insertion and extraction. However, the first discharge capacity of LTNMCO was 123.1 and 94.7 mAh·g$^{-1}$ at 0.1C and 10C rates, respectively, with a retention rate of 76.96%, much higher than those of the other three samples. It is mainly the Ti–Cr codoping that plays a synergistic role. Ti stabilizes the surface structure of the electrode by forming a Ti–O oxide on the surface, which is hardly eroded by the electrolyte, and isolates the LNMO grain surface from the electrolyte, while Cr doping reduces the content of $Mn^{3+}$ and suppresses the dissolution of Mn and the distortion of the material.[30,44] Moreover, the smooth and clean surface formed by TiCr doping is beneficial to prevent this undesirable reaction. In
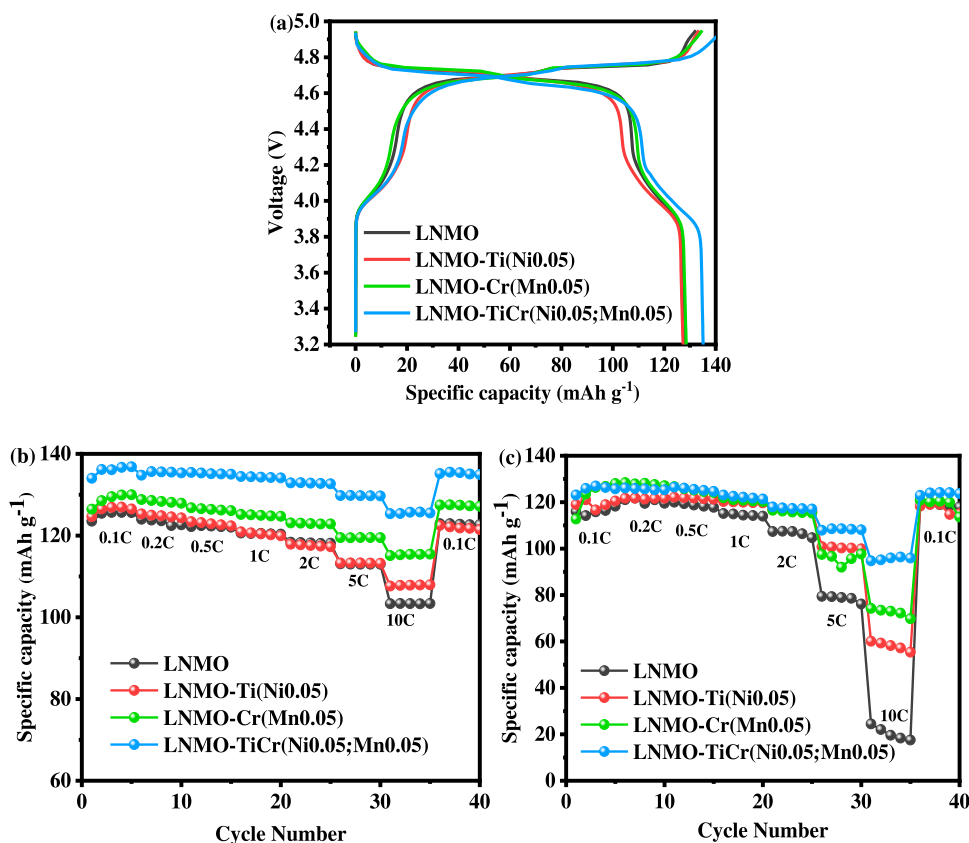
**Figure 5.** (a) 0.2C First cycle curves, (b) room-temperature rate curves, and (c) high-temperature rate curves for LNMO, LNMO-Ti(Ni0.05), LNMO-Cr(Mn0.05), and LNMO-TiCr(Ni0.05; Mn0.05) materials.
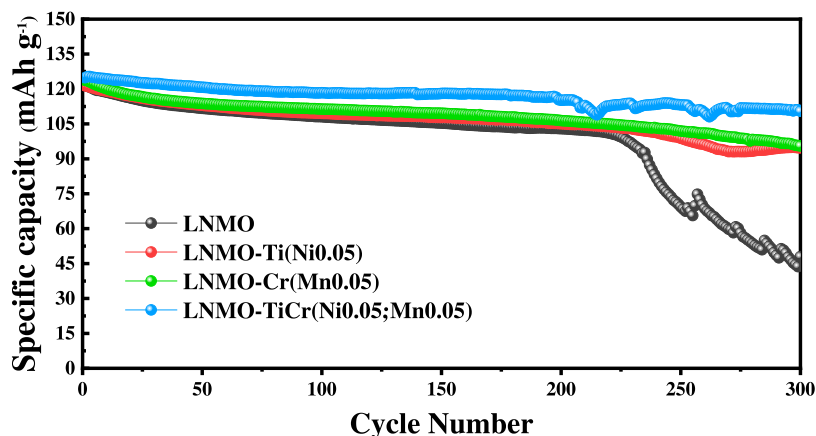


**Figure 6.** 1C Rate cycle performance curves for LNMO, LNMO-Ti(Ni0.05), LNMO-Cr(Mn0.05), and LNMO-TiCr(Ni0.05; Mn0.05) materials.

short, maintaining a stable interface is the key to LTNMCO's good rate performance.

To evaluate the stability of the electrode during a long cycle, the material was subjected to a constant current charge/discharge test at room temperature with a voltage setting range of 3.2−4.95 V and 300 cycles at a 1C rate. Figure 6 shows the cycling performance curves of four samples at 1C. The starting discharge capacities of LNMO, LTNMO, LNMCO, and LTNMCO are 121.4, 121.4, 123.7, and 124.8 mAh·$g^{-1}$, respectively, and the discharge capacities and capacity retention rates decrease differently as the cycles proceeded. After 300 cycles, the remaining discharge capacities of the four materials are 48.0, 94.7, 95.5, and 110.4 mAh·$g^{-1}$, and the

capacity retention rates were 39.53, 78.02, 77.20, and 88.47%, respectively. As a result, the LTNMCO achieves excellent cycling properties and remains stable after long cycling times. Although spinel materials are known to be less prone to phase changes than other cathodes, it is still difficult to maintain structural stability over long cycles due to high voltages and the formation of SEI films. The strong bonding of Ti−O and Cr−O can facilitate the formation of excellent morphology and enhance the structural stability of the material. In addition, the synergistic effect of Ti−Cr can also optimize the amount of $Mn^{3+}$ in the material to improve the electrochemical performance as well as inhibit structural distortion and capacity degradation during long cycles. The working
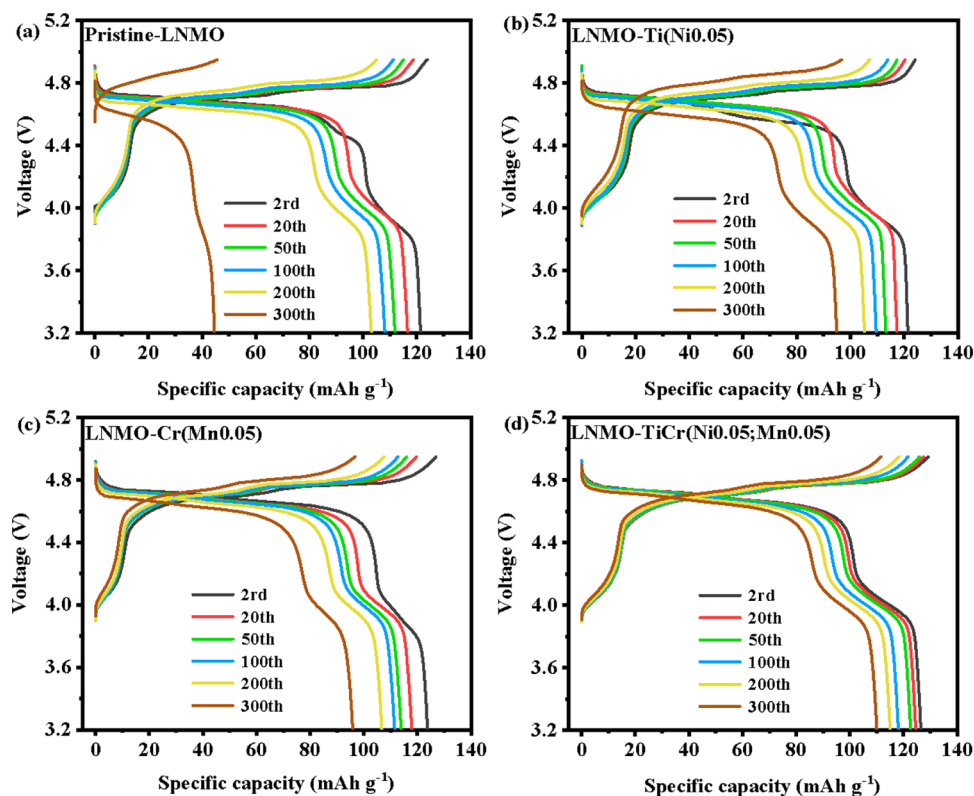
**Figure 7.** Charge−discharge curves of materials in the 2nd, 20th, 50th, 100th, 200th, and 300th cycle of (a) pristine LNMO, (b) LNMO-Ti(Ni0.05), (c) LNMO-Cr(Mn0.05), and (d) LNMO-TiCr(Ni0.05;Mn0.05).
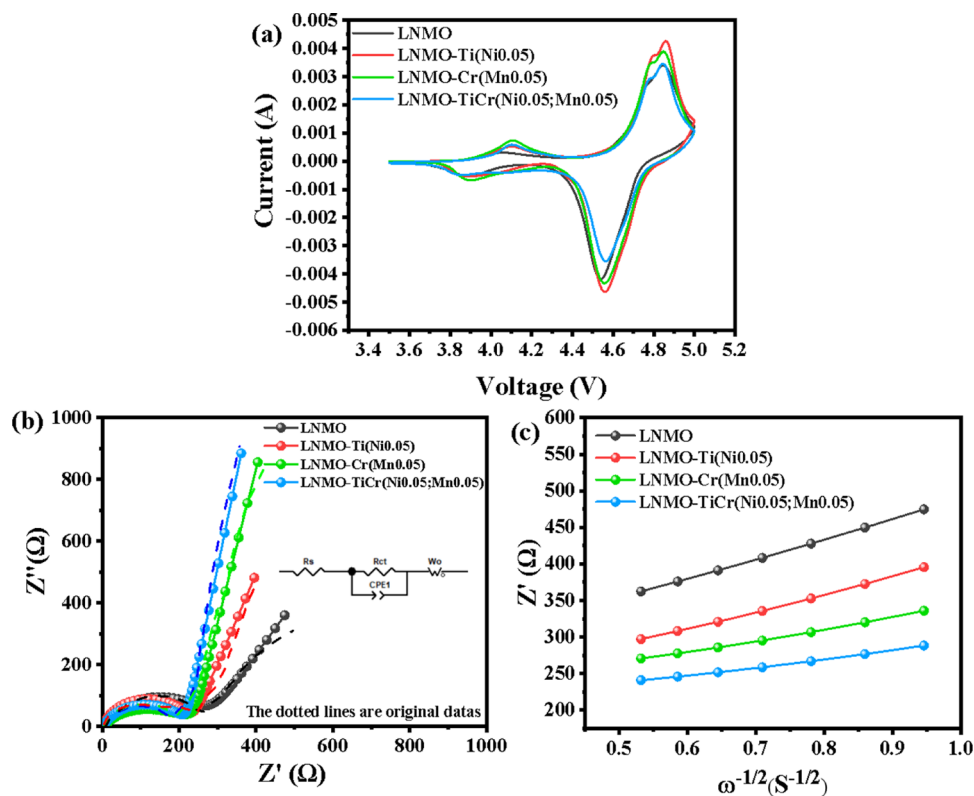


**Figure 8.** (a) CV curves and (b) electrochemical impedance spectra (c) $Z$-$\omega^{-1/2}$ of LNMO, LNMO-Ti(Ni0.05), LNMO-Cr(Mn0.05), and LNMO-TiCr(Ni0.05;Mn0.05) materials.

condition of the material is further observed by the charging and discharging curves with different numbers of cycles. Figure

7a−d shows the charge/discharge curves for all materials at the 2nd, 20th, 50th, 100th, 200th, and 300th cycle. Pristine

**Table 3. CV Parameters for LNMO, LNMO-Ti(Ni0.05), LNMO-Cr(Mn0.05), and LNMO-TiCr(Ni0.05; Mn0.05) Materials**

| sample | OP potential/V | RP potential/V | $\Delta E$/V | $I_{pa}$/mA | $I_{pc}$/mA | $I_{pa}/I_{pc}$ | $D_{Li}$/cm$^2\cdot$s$^{-1}$ |
|---|---|---|---|---|---|---|---|
| LNMO | 4.847 | 4.539 | 0.308 | 3.41 | 4.18 | 0.816 | $8.61 \times 10^{-14}$ |
| LTNMO | 4.856 | 4.562 | 0.294 | 4.25 | 4.63 | 0.918 | $1.154 \times 10^{-13}$ |
| LNMCO | 4.848 | 4.561 | 0.287 | 3.88 | 4.32 | 0.898 | $2.642 \times 10^{-13}$ |
| LTNMCO | 4.843 | 4.562 | 0.281 | 3.46 | 3.55 | 0.975 | $4.946 \times 10^{-13}$ |

LNMO has a very short charge/discharge voltage plateau after 300 cycles and is almost impossible to work correctly. Although the single-element doping maintains the stability of the working voltage plateau, there is a significant decrease in capacity and voltage. Whereas the synergistic effect played by Ti−Cr doping makes the capacity and voltage of LTNMCO decay little after the cycle, maintaining a high energy density.

The CV and EIS tests are used to analyze the chemical state of the material after doping. As shown in Figure 8a, all samples have symmetric redox peaks near 4.0 and 4.7 V. The weak peak near 4.0 V is the $Mn^{3+}/Mn^{4+}$ redox peak, which is in agreement with the previous analysis, and the strong split peaks near 4.7 V can be assigned to the redox peaks of $Ni^{2+}/Ni^{3+}$ and $Ni^{3+}/Ni^{4+}$. It is suggested that the capacity of the material is mainly derived from the $Ni^{2+}/Ni^{4+}$ redox couple.[45] The specific CV data for the four samples are presented in Table 3. The potential difference between oxidation and reduction peaks (marked as $\Delta E$) of LNMO, LTNMO, LNMCO, and LTNMCO is 0.308, 0.294, 0.287, and 0.281 V, respectively, reflecting that the element doping can effectively reduce the polarization effect.[46] Moreover, the ratio of oxidation peak current $I_{pa}$ and reduction peak current $I_{pc}$ for LTNMCO is 0.975, which is the highest among the four samples, indicating more reversible performance and stability over long cycles and high rate tests. The resistance and Li$^+$ ion insertion/extraction kinetics of the material are investigated by EIS. The Nyquist and equivalent circuit graphs are shown in Figure 8b. All samples consist of a semicircle in the mid-frequency region corresponding to charge transfer resistance ($R_{ct}$) and a straight line in the low-frequency region. The pristine LNMO material has the largest diameter, and the $R_{ct}$ of LNMO, LTNMO, LNMCO, and LTNMCO is 258.3, 214.4, 210.9, and 205.6 Ω, respectively. The lithium-ion diffusion coefficient $D_{Li}$ of the material can be calculated by the slope of the straight line in the low-frequency region using the following equation[47,48]

$$D_{Li} = (R^2 T^2)/(2n^2 F^4 A^2 C_{Li}^{2} \sigma^2) \qquad (1)$$

where $R$ is the gas constant (8.314 JK$^{-1}$ mol$^{-1}$), $T$ is the absolute temperature (298 K), $n$ is the number of electrons transferred per mole of a substance in the half-reaction, $F$ is the Faraday constant (96500 C/mol), $A$ is the electrode area, $C_{Li}$ is the lithium-ion concentration, and $\sigma$ is the slope of the fit according to the Warburg factor, fulfilling the following equation[48]

$$Z' = R_{ct} + R_s + \sigma \omega^{-1/2} \qquad (2)$$

The fitted $Z'$ vs $-\omega^{-1/2}$ is shown in Figure 8c, and the calculated $D_{Li}$ of LNMO, LTNMO, LNMCO, and LTNMCO is listed in Table 3. As a result, LTNMCO has the best electrochemical performance with the lowest charge transfer resistance and the highest diffusion coefficient of lithium ions. The enhanced performance may be probably because the Ti−Cr codoping reduces the polarization effect and thus reduces the impedance; in addition, the doped material increases a certain amount of $Mn^{3+}$, which promotes the diffusion of lithium ions to improve the electrical conductivity.

## 4. CONCLUSIONS

In summary, Ti, Cr single-doped and Ti−Cr codoped LiNi$_{0.5}$Mn$_{1.5}$O$_4$ cathode materials were prepared by a simple solid-phase method. The effects of Ti and Cr elements on the structure, morphology, and electrochemical properties of the material have been systematically investigated. Ti, Cr was successfully doped into the LiNi$_{0.5}$Mn$_{1.5}$O$_4$ structure and the material keeps the $Fd\bar{3}m$ space group structure with an increase in the lattice parameters and cationic disorder of the material. The obtained LTNMCO cathode material has high capacity and good cycling and rate performances, since the doping Ti element can stabilize the structure of the material and inhibit the formation of impure phases, while the Cr element can slow down the dissolution of the metal and reduce the Jahn−Teller phenomenon. Moreover, the synergistic effect of TiCr ions improves the content of $Mn^{3+}$ ions in the material and helps grow smooth and clean surfaces of grains. The LNMO-TiCr(Ni0.05; Mn0.05) material exhibits excellent electrochemical properties with reduced interfacial resistances and increased ionic conductivity, which would give a good sight for the study of high-voltage LNMO cathode materials.

## ■ AUTHOR INFORMATION

**Corresponding Authors**

    **Cuilian Wen** − *Multiscale Computational Materials Facility, and Key Laboratory of Eco-materials Advanced Technology, College of Materials Science and Engineering, Fuzhou University, Fuzhou 350100, P. R. China;* orcid.org/0000-0002-0410-606X; Email: clwen@fzu.edu.cn

    **Hengyi Li** − *Fujian Applied Technology Engineering Center of Power Battery Materials, Fujian College of Water Conservancy and Electric Power, Sanming 366000, P. R. China;* Email: henryzxm1986@126.com

    **Zhengbing Xu** − *State Key Laboratory of Featured Metal Materials and Life-cycle Safety for Composite Structures, Guangxi University, Nanning 530004, P. R. China; Centre of Ecological Collaborative Innovation for Aluminum Industry in Guangxi, Guangxi University, Nanning 530004, P. R. China;* Email: xuzhb@gxu.edu.cn

**Authors**

    **Yiyuan Luo** − *State Key Laboratory of Featured Metal Materials and Life-cycle Safety for Composite Structures, Guangxi University, Nanning 530004, P. R. China; Centre of Ecological Collaborative Innovation for Aluminum Industry in Guangxi, Guangxi University, Nanning 530004, P. R. China; Sanming New Energy Industry Technology Institute, Sanming 365007, P. R. China;* orcid.org/0009-0000-6764-2815

    **Zhou Cui** − *Multiscale Computational Materials Facility, and Key Laboratory of Eco-materials Advanced Technology,*

College of Materials Science and Engineering, Fuzhou University, Fuzhou 350100, P. R. China

**Changxu Wu** − *Multiscale Computational Materials Facility, and Key Laboratory of Eco-materials Advanced Technology, College of Materials Science and Engineering, Fuzhou University, Fuzhou 350100, P. R. China*

**Baisheng Sa** − *Multiscale Computational Materials Facility, and Key Laboratory of Eco-materials Advanced Technology, College of Materials Science and Engineering, Fuzhou University, Fuzhou 350100, P. R. China;* ⓘ orcid.org/0000-0002-9455-7795

**Jianping Huang** − *Sanming New Energy Industry Technology Institute, Sanming 365007, P. R. China*

**Chao Xu** − *Xiamen Talentmats New Materials Science & Technology Co., Ltd., Xiamen, Fujian 361015, P. R. China*

Complete contact information is available at:
https://pubs.acs.org/10.1021/acsomega.3c01524

## Notes

The authors declare no competing financial interest.

## ■ REFERENCES

(1) Manthiram, A.; Chemelewski, K.; Lee, E. S. A perspective on the high-voltage LiMn1.5Ni0.5O4 spinel cathode for lithium-ion batteries. *Energy Environ. Sci.* **2014**, *7*, 1339−1350.

(2) Kim, J. H.; Pieczonka, N. P. W.; Yang, L. Challenges and Approaches for High-Voltage Spinel Lithium-Ion Batteries. *ChemPhysChem* **2014**, *15*, 1940−1954.

(3) Fang, H. S.; Wang, Z. X.; Li, X. H.; Guo, H. J.; Peng, W. J. Exploration of high capacity LiNi0.5Mn1.5O4 synthesized by solid-state reaction. *J. Power Sources* **2006**, *153*, 174−176.

(4) Yi, T. F.; Mei, J.; Zhu, Y. R. Key strategies for enhancing the cycling stability and rate capacity of LiNi0.5Mn1.5O4 as high-voltage cathode materials for high power lithium-ion batteries. *J. Power Sources* **2016**, *316*, 85−105.

(5) Liu, W. J.; Shi, Q.; Qu, Q.; et al. Improved Li-ion diffusion and stability of a LiNi0.5Mn1.5O4 cathode through in situ co-doping with dual-metal cations and incorporation of a superionic conductor. *J. Mater. Chem. A* **2017**, *5*, 145−154.

(6) Park, S. H.; et al. Comparative study of different crystallographic structure of LiNi0.5Mn1.5O4-delta cathodes with wide operation voltage (2.0-5.0 V). *Electrochim. Acta* **2007**, *52*, 7226−7230.

(7) Haridas, A. K.; Sharma, C. S.; Rao, T. N. Caterpillar-like sub-micron LiNi0.5Mn1.5O4 structures with site disorder and excess Mn3+ as high performance cathode material for lithium ion batteries. *Electrochim. Acta* **2016**, *212*, 500−509.

(8) Kim, J. H.; Myung, S. T.; Yoon, C. S.; Kang, S. G.; Sun, Y. K. Comparative Study of LiNi0.5Mn1.5O4-δ and LiNi0.5Mn1.5O4 Cathodes Having Two Crystallographic Structures: *Fd*3*m* and P4332. *Chem. Mater.* **2004**, *16*, 906−914.

(9) Zhong, Q.; Bonakdarpour, A.; Zhang, M.; Gao, Y. Synthesis and electrochemistry of LiNiMnO4. 1997.

(10) Chen, Y.; Sun, Y.; Huang, X. Origin of the Ni/Mn ordering in high-voltage spinel LiNi0.5Mn1.5O4: The role of oxygen vacancies and cation doping. *Comput. Mater. Sci.* **2016**, *115*, 109−116.

(11) Zhu, R. N.; Zhang, S.; Guo, Q.; et al. More than just a protection layer: Inducing chemical interaction between Li3BO3 and

LiNi0.5Mn1.5O4 to achieve stable high-rate cycling cathode materials. *Electrochim. Acta* **2020**, *342*, No. 136074.

(12) Kim, M. C.; Lee, Y. W.; Pham, T. K.; Sohn, J. I.; Park, K. W. Chemical valence electron-engineered LiNi0.4Mn1.5MtO4 (M-t = Co and Fe) cathode materials with high-performance electrochemical properties. *Appl. Surf. Sci.* **2020**, *504*, No. 144514.

(13) Pieczonka, N. P. W.; Liu, Z.; Lu, P.; et al. Understanding Transition-Metal Dissolution Behavior in LiNi0.5Mn1.5O4 High-Voltage Spinel for Lithium Ion Batteries. *J. Phys. Chem. C* **2013**, *117*, 15947−15957.

(14) Li, S. R.; Chen, C. H.; Xia, X.; Dahn, J. R. The Impact of Electrolyte Oxidation Products in LiNi0.5Mn1.5O4/Li4Ti5O12 Cells. *J. Electrochem. Soc.* **2013**, *160*, A1524−A1528.

(15) Sun, P.; Ma, Y.; Zhai, T. Y.; Li, H. Q. High performance LiNi0.5Mn1.5O4 cathode by Al-coating and Al3+-doping through a physical vapor deposition method. *Electrochim. Acta* **2016**, *191*, 237−246.

(16) Okudur, F. U.; et al. Ti surface doping of LiNi0.5Mn1.5O4-delta positive electrodes for lithium ion batteries. *RSC Adv.* **2018**, *8*, 7287−7300.

(17) Liu, M. H.; Huang, H. T.; Lin, C. M.; Chen, J. M.; Liao, S. C. Mg gradient-doped LiNi0.5Mn1.5O4 as the cathode material for Li-ion batteries. *Electrochim. Acta* **2014**, *120*, 133−139.

(18) Mao, J.; Dai, K.; Xuan, M.; et al. Effect of Chromium and Niobium Doping on the Morphology and Electrochemical Performance of High-Voltage Spinel LiNi0.5Mn1.5O4 Cathode Material. *ACS Appl. Mater. Interfaces* **2016**, *8*, 9116−9124.

(19) Yoon, J.; Jeong, M.; Bae, I. T.; Nam, K. W.; Yoon, W. S. Zr-doping effect on the capacity retention of LiNi0.5Mn1.5O4-delta cycled between 5.0 and 1.0 V: In situ synchrotron X-Ray diffraction study. *J. Power Sources* **2017**, *368*, 1−10.

(20) Lin, F. C.; Wu, H.; Chen, T.; et al. The Cu-Y co-doping LiNi0.5Mn1.5O4 with modified morphology and enhanced electrochemical property for a 5 V lithium-ion battery. *J. Mater. Sci.: Materi. Electron.* **2022**, *33*, 283−297.

(21) Wei, A. J.; Mu, J.; He, R.; et al. Enhanced Electrochemical Performance of LiNi0.5Mn1.5O4 Composite Cathodes for Lithium-Ion Batteries by Selective Doping of K+/Cl- and K+/F. *Nanomaterials* **2021**, *11*, No. 2323.

(22) Kim, D. W.; et al. Metastable oxysulfide surface formation on LiNi0.5Mn1.5O4 single crystal particles by carbothermal reaction with sulfur-doped heterocarbon nanoparticles: new insight into their structural and electrochemical characteristics, and their potential applications. *J. Mater. Chem. A* **2020**, *8*, 22302−22314.

(23) Wei, A. J.; Mu, J.; He, R.; et al. Li+ and Cl- co-doped LiNi0.5Mn1.5O4 cathode material with truncated octahedral shape and enhanced electrochemical performance for Li-ion batteries. *Solid State Ion.* **2021**, *371*, No. 115753.

(24) Chen, A.; Kong, L.; Shu, Y.; Yan, W.; Wu, W.; Xu, Y.; et al. Role of al-doping with different sites upon the structure and electrochemical performance of spherical lini0.5mn1.5o4 cathode materials for lithium-ion batteries. *RSC Adv.* **2019**, *9*, 12656−12666.

(25) Li, S.; Wei, Y.; Wang, P.; et al. Synergism of Cu and al co-doping on improvements of structural integrity and electrochemical performance for lini0.5mn1.5o4. *J. Alloys Compd.* **2020**, *820*, No. 153140.

(26) Wei, A.; Li, W.; Chang, Q.; Bai, X.; He, R.; et al. Effect of mg2+/f- co-doping on electrochemical performance of lini0.5mn1.5o4 for 5 v lithium-ion batteries. *Electrochim. Acta* **2019**, *323*, No. 134692.

(27) Chemelewski, K. R.; Lee, E. S.; Li, W.; Manthiram, A. Factors Influencing the Electrochemical Properties of High-Voltage Spinel Cathodes: Relative Impact of Morphology and Cation Ordering. *Chem. Mater.* **2013**, *25*, 2890−2897.

(28) Lu, D.; et al. Failure mechanism for high voltage graphite/LiNi0.5Mn1.5O4 (LNMO) Li-ion cells stored at elevated temperature 28. *J. Electroanal. Chem.* **2015**, *758*, 33−38.

(29) Liu, G. Q.; Du, Y. L.; Liu, W. B.; Wen, L. Study on the action mechanism of doping transitional elements in spinel LiNi0.5Mn1.5O4. *Electrochim. Acta* **2016**, *209*, 308−314.

(30) Wang, J.; et al. High-Voltage LiNi0.45Cr0.1Mn1.45O4 Cathode with Superlong Cycle Performance for Wide Temperature Lithium-Ion Batteries. *Adv. Funct. Mater.* **2018**, *28*, No. 1704808.

(31) Lim, J. M.; Oh, R. G.; Kim, D.; et al. Design of Surface Doping for Mitigating Transition Metal Dissolution in LiNi0.5Mn1.5O4 Nanoparticles. *ChemSusChem* **2016**, *9*, 2967−2973.

(32) Wang, L.; Chen, D.; Wang, J.; et al. Improved structural and electrochemical performances of LiNi0.5Mn1.5O4 cathode materials by Cr3+ and/or Ti4+ doping. *RSC Adv.* **2015**, *5*, 99856−99865.

(33) Hsu, S. C.; Hsiao, Y. S.; Lu, C. Z.; et al. The effect of dual-doping on the electrochemical performance of LiNi0.5Mn1.5O4 and its application in full-cell lithium-ion batteries. *Ceram. Int.* **2022**, *48*, 14778−14788.

(34) Sun, H. Y.; Kong, X.; Wang, B. S.; Luo, T. B.; Liu, G. Y. LiNi0.5Mn1.45Zn0.05O4 with Excellent Electrochemical Performance for Lithium Ion Batteries. *Int. J. Electrochem. Sci.* **2017**, *12*, 8609−8621.

(35) Song, J.; et al. Role of oxygen vacancies on the performance of Li [Ni0. 5−x Mn1. 5+ x] O4 (x = 0, 0.05, and 0.08) spinel cathodes for lithium-ion batteries 34. *Chem. Mater.* **2012**, *24*, 3101−3109.

(36) Zheng, J.; et al. Enhanced Li+ ion transport in LiNi 0.5 Mn 1.5 O 4 through control of site disorder 35. *Phys. Chem. Chem. Phys.* **2012**, *14*, 13515−13521.

(37) Risthaus, T.; et al. Synthesis of spinel LiNi0. 5Mn1. 5O4 with secondary plate morphology as cathode material for lithium ion batteries 36. *J. Power Sources* **2015**, *293*, 137−142.

(38) Momma, K.; Izumi, F. VESTA 3 for three-dimensional visualization of crystal, volumetric and morphology data 37. *J. Appl. Crystallogr.* **2011**, *44*, 1272−1276.

(39) Chang, Q.; Wei, A.; Li, W.; et al. Structural and electrochemical characteristics of Al2O3-modified LiNi0.5Mn1.5O4 cathode materials for lithium-ion batteries. *Ceram. Int.* **2019**, *45*, 5100−5110.

(40) Bao, S. J.; Li, C. M.; Li, H. L.; Luong, J. H. T. Morphology and electrochemistry of LiMn2O4 optimized by using different Mn-sources. *J. Power Sources* **2007**, *164*, 885−889.

(41) Yi, T. F.; Li, C. Y.; Zhu, Y. R.; Shu, J.; Zhu, R. S. Comparison of structure and electrochemical properties for 5 V LiNi0.5Mn1.5O4 and LiNi0.4Cr0.2Mn1.4O4 cathode materials. *J. Solid State Electrochem.* **2009**, *13*, 913−919.

(42) Zhou, L.; Zhao, D.; Lou, X. W. Lini0.5mn1.5o4 hollow structures as high-performance cathodes for lithium-ion batteries. *Angew. Chem., Int. Ed.* **2012**, *51*, 239−241.

(43) Pang, W. K.; Lu, C. Z.; Liu, C. E.; et al. Crystallographic origin of cycle decay of the high-voltage LiNi0.5Mn1.5O4 spinel lithium-ion battery electrode. *Phys. Chem. Chem. Phys.* **2016**, *18*, 17183−17189.

(44) Kim, J.-H.; et al. In Situ Formation of a Cathode−Electrolyte Interface with Enhanced Stability by Titanium Substitution for High Voltage Spinel Lithium-Ion Batteries 39. *Adv. Mater. Interfaces* **2015**, *2*, No. 1500109.

(45) Kim, J. H.; Huq, A.; Chi, M.; et al. Integrated Nano-Domains of Disordered and Ordered Spinel Phases in LiNi0.5Mn1.5O4 for Li-Ion Batteries. *Chem. Mater.* **2014**, *26*, 4377−4386.

(46) Oh, S. H.; Chung, K. Y.; Jeon, S. H.; et al. Structural and electrochemical investigations on the LiNi0.5-xMn1.5-yMx+yO4 (M = Cr, Al, Zr) compound for 5 V cathode material. *J. Alloys Compd.* **2009**, *469*, 244−250.

(47) Cho, H. M.; Chen, M. V.; MacRae, A. C.; Meng, Y. S. Effect of Surface Modification on Nano-Structured LiNi0.5Mn1.5O4 Spinel Materials. *ACS Appl. Mater. Interfaces* **2015**, *7*, 16231−16239.

(48) Yi, T. F.; Xie, Y.; Wu, Q.; et al. High rate cycling performance of lanthanum-modified Li4Ti5O12 anode materials for lithium-ion batteries. *J. Power Sources* **2012**, *214*, 220−226.